Deep-sea Research Part I-oceanographic Research Papers
April 2016, Volume 110 Pages 20-32
https://doi.org/10.1016/j.dsr.2015.12.007
https://archimer.ifremer.fr/doc/00302/41354/

Acoustic micronektonic distribution is structured by macroscale oceanographic processes across 20–50°S latitudes in the South-Western Indian Ocean

Béhagle Nolwenn [1, 2, *], Cotte Cédric [3], Ryan Tim E. [4], Gauthier Olivier [5], Roudaut Gildas [1], Brehmer Patrice [6], Josse Erwan [1], Cherel Yves [7]

[1] CNRS IRD IFREMER UBO, IRD, UMR LEMAR 6539, BP70, F-29280 Plouzane, France.
[2] CNRS IRD MNHN UPMC, CNRS, UMR LOCEAN 7159, 4 Pl Jussieu, F-75005 Paris, France.
[3] CNRS IRD MNHN UPMC, MNHN, UMR LOCEAN 7159, 4 Pl Jussieu, F-75005 Paris, France.
[4] CSIRO, Wealth Oceans Flagship, Marine & Atmospher Res, GPO Box 1538, Hobart, Tas 7001, Australia.
[5] CNRS IRD IFREMER UBO, UMR LEMAR 6539, UBO, F-29280 Plouzane, France.
[6] CNRS IRD IFREMER UBO, IRD, UMR LEMAR 195, Ctr Rech ISRA Hann PRH CRODT, Dakar, Senegal.
[7] Univ Rochelle, CNRS, UMR CEBC 7372, F-79360 Villiers En Bois, France.

* Corresponding author : Nolwenn Béhagle, email address : nolwenn.behagle@ird.fr

Abstract :

Micronekton constitutes the largest unexploited marine biomass worldwide. It is one of the most conspicuous and ecologically important components of the still poorly known mesopelagic ecosystem. Acoustic data were collected from both fishing and research vessels along 18 transects for a total of 47 682 linear kilometers to investigate large-scale distribution of micronekton over a long latitudinal gradient (20–50 °S) and two contrasted seasons (summer and winter) in the South-Western Indian Ocean. Acoustic backscatter at 38 kHz was used as a proxy of mid-water organisms' abundance (0–800 m depth). Two consistent features were diel vertical migration of backscatters and vertical distribution of micronekton in three distinct layers, namely the surface (SL), intermediate (IL) and deep (DL) layers. Satellite remote sensing data was used to position oceanic fronts, and hence define water masses, from the tropical to low Antarctic zones. A key finding of this study was the significant correlation observed between abundance and distribution of acoustic backscatter and position relative to these front and water masses. Total backscatter peaked in the subtropical zone, with low abundances in the colder Polar Frontal Zone. The high overall abundances in subtropical waters resulted mainly from high backscatters in the IL and DL that contrasted with low SL values, especially during the day (2–11%). The warmer the waters, the higher SL backscatter was, with the highest absolute and relative (38–51% of the total abundance) values observed at night in the Tropical Zone and the lowest abundance in the Antarctic Zone. No significant seasonal pattern was found, but SL backscatters were very low in winter compared to summer in the Polar Frontal Zone. Moreover, the Northern winter shift of the fronts induced a Northern latitudinal shift of the peak in abundance from summer to winter. The present study highlights the value of building large acoustic databases collected from both research and fishing vessels. The method provides unique

opportunities to gather basic information on micronekton and is an essential step to describe oceanic zones of relevant biological interest in terms of trophic ecology.

Highlights

► Acoustic data (38 kH) characterizing micronekton were repeatedly collected over 10–800 m depth across a large latitudinal gradient (20–50°S) in the Indian Ocean. ► A strong correlation was evidenced between spatial distribution of micronekton and macroscale oceanography (water masses delineated by fronts). ► Micronektonic abundance overall peaked in the subtropics. ► The vertical structure of micronektonic abundance varied according to water masses. ► No major seasonal (summer versus winter) difference was found.

Keywords : Mesopelagic, Acoustics, Mid-water organisms, Water masses, Southern Ocean

1. Introduction

Overall catches of coastal and offshore fisheries have decreased since the mid-1990s, with 32% of stocks considered overexploited, depleted or recovering from depletion and a further 53% exploited at maximum capacity (FAO, 2010). Micronekton are relatively small organisms, ~2-20 cm in length (Kloser et al., 2009), that occur worldwide and include small pelagic fishes, cephalopods, crustaceans and gelatinous animals. While they currently constitute a barely harvested marine biomass resource, micronektonic organisms are being seriously considered for commercial exploitation in the near future (*e.g.,* Menon, 2004; Catul et al., 2011; Nicol et al. 2012). Indeed, they form a substantial biomass (*e.g.* 379 million tons of Antarctic krill in Antarctic waters, and ~1 to 10 billion tons of mid-water fish worldwide; Atkinson et al., 2009; Irigoien et al., 2014) with high nutritional value for human consumption (Shaviklo and Rafipour, 2013; Koizumi et al., 2014). Most micronektonic species occur in oceanic waters, where they form one of the most conspicuous and ecologically important components of the vast and still poorly known mesopelagic zone (200-1000 m depth). Indeed, micronekton plays an important role in the export of carbon from the surface to mesopelagic depths (the biological pump) through its extensive daily vertical migrations to feed near the surface at night and hide from large predators at mesopelagic depths during the day (Bianchi et al., 2013). It plays a prominent role in oceanic food webs by providing a critical intermediate link between primary-trophic level organisms and top predators, including commercially targeted fish species and oceanic squids, as well as charismatic and endangered marine mammals and seabirds (Rodhouse and Nigmatullin, 1996; Robertson and Chivers, 1997; Potier et al. 2007; Spear et al. 2007).

Despite their ecological importance, relatively scant attention has been paid to mid-trophic level organisms in comparison to phytoplankton and top consumers (Handegard et al.,

2013). Pelagic trawling is the traditional method to scientifically collect micronekton and it offers the advantage of allowing both precise taxonomic identification and size measurement of catches. However, it induces two main biases. First, avoidance and escape from pelagic trawls result in underestimations of micronekton biomass, which can reach an order of magnitude or more for mid-water fishes (Kloser et al., 2009; Pakhomov and Yamamura, 2010; Kaartvedt et al., 2012). Second, as catches covering the depth spectrum and both day and night are necessary to provide an accurate description of micronekton distribution trawling operations are costly and time consuming and hence generally limited in time and space. In contrast, fisheries acoustics (hereafter acoustics) provide a cost and time efficient tool for monitoring micronekton due to the (i) simultaneous recording of its horizontal and vertical structure at fine spatial scales, and (ii) negligible behavioural effects on the targeted animals. While mono-frequency acoustics do not allow taxonomic identification, it can be used over large spatial and temporal scales, with dedicated research vessels as well as opportunistic fishing vessels (Karp, 2007; Kloser et al., 2009).

In the South-Western Indian Ocean, the importance of micronekton is illustrated by the large populations of Sub-Antarctic seabirds and pinnipeds that prey primarily on schooling myctophids and swarming euphausiids and hyperiids (Cooper and Brown, 1990; Woehler and Green, 1992; Guinet et al., 1996; Bocher et al., 2001). However, to our knowledge, acoustic characterization of micronekton in the area is limited to surveys conducted in the vicinity of the sub-Antarctic Prince Edward Islands (Miller, 1982; Perissinotto and McQuaid 1992; Pakhomov and Froneman, 1999) and Heard Island (Bedford et al., 2015) and to mesoscale investigations in the tropical Mozambique Channel (Sabarros et al., 2009; Béhagle et al., 2014). Mesoscale oceanographic features are known to influence biological features (Sabarros et al., 2009; Godø et al., 2012), but few investigations have been conducted at larger spatial scales (O'Driscoll et al., 2011; Fielding et al. 2012). The macroscale oceanography of the

South-Western Indian Ocean has been characterized (Park and Gamberoni, 1995; Stramma and Lutjeharms, 1997; Pollard and Read, 2001), with well-defined oceanic fronts constituting biogeographical boundaries delimiting relatively homogenous oceanic zones (Pakhomov and McQuaid, 1996; Koubbi et al., 2011; Commins et al., 2014).

The main goal of the present work was to use acoustic data collected from both research and opportunistic fishing vessels to investigate large-scale distribution patterns of micronekton in the South-Western Indian Ocean. Micronekton distribution was characterized at various spatial and temporal scales with acoustic backscatter at 38 kHz (Escobar-Flores et al., 2013; Béhagle et al. 2014). Our objectives were three-fold. Firstly, micronekton distribution within the top 800 m of the water column was analyzed to verify whether these pelagic organisms were vertically structured in distinct depth layers and underwent daily vertical migration (Benoit-Bird et al., 2009; Escobar-Flores et al., 2013; Béhagle et al., 2014). Secondly, and more importantly, the structuring effect of latitudes and then of macroscale oceanography on micronekton distribution and abundance was investigated over a large latitudinal gradient, from the tropics to Antarctic waters (20-50°S, 50-80°E). Finally, considering that the latitudinal position of fronts vary with seasons (Kim and Orsi, 2014) and seasonality varies with latitudes, horizontal and vertical structures of mid-water organisms were compared between two contrasted seasons; summertime and wintertime, in order to test the hypothesis that seasonal differences should be more marked at higher than lower latitudes (Moore and Abbott, 2000; Hunt and Hosie, 2006; Flores et al., 2014).

2. Materials and methods

Two different sources of acoustic data collected in the South-Western Indian Ocean (20-60°S, 50-80°E) were used in this investigation. Firstly, fishing trips carried out from 2010 to

2013 within the Australian Integrated Marine Observing System - Bio-Acoustic Ship Of Opportunity Program (IMOS-BASOOP). This program was initiated in 2010 with the main goal of collecting opportunistic acoustic data using transiting commercial and research vessels. Secondly, research surveys carried out from 2013 to 2014 within MyctO-3D-MAP (Myctophid assessment in relation to oceanographic conditions: a three dimension density distribution approach combining modelling-, acoustic- and predators' data). The MyctO-3D-MAP programme aims to collect and analyze information on the distribution and habitat of mesopelagic fish using various non-conventional (bio-logging and predators as samplers of marine ecosystems) and conventional methods, including acoustics. IMOS-BASOOP and MyctO-3D-MAP data complement each other and, combined, they provide a large database with extensive spatiotemporal coverage of the study area (Fig. 1, Table 1).

In all cases, acoustic data were collected using split-beam echo sounders operating at one (38 kHz) or two (38 and 120 kHz) frequencies (Table 2). Since low frequencies have greater detection ranges than high frequencies (MacLennan and Simmonds, 1992), a 38 kHz accoustic signal allowed for collecting data on a vertical range from 10 to 800 m depth compared to one of 10 to 300 m depth for a 120 kHz signal. During each survey, the cruise path was divided into several linear transects (Table 1) using the following criteria: (i) data quality (based on the amount of acoustic interference), (ii) cruise latitudinal range, with the longest transects favored, (iii) optimal vessel speed (between 6 and 16 knots), (iv) bottom depth (≥ 1000 m; hence, in the oceanic domain), and (v) linearity of the transects *i.e.* linear transects were favored and redundant data were removed.

The full dataset covers 47 682 km of acoustic recording in oceanic waters from n=18 transects conducted during the IMOS-BASOOP (n = 12; 31 290 km) and MyctO-3D-MAP (n = 6; 16 392 km) programs. The dataset includes both summer (n = 11; 27 805 km) and winter (n = 7; 19 877 km) transects from tropical to low Antarctic waters (Fig. 1, Table 1).

2.1. IMOS-BASOOP acoustic data collection and processing

Using commercial fishing vessels as research vessels (Godø et al., 2014), twelve transects from the IMOS-BASOOP dataset were analyzed (Table 1, Fig. 1). Data collection, management and processing procedures are detailed in Ryan (2011). Data were recorded continuously (both day and night) using a Simrad ES60 or ES70 split-beam echo sounder at 38 kHz. The depth of the hull-mounted acoustic transducer was 6 or 7 m below sea surface, depending on the vessels. Hence, an offset of 10 m below the surface was used to account for the depth of the transducer and acoustic interference from surface turbulence. The echosounder systems were calibrated following the procedures recommended in Foote et al. (1987). Settings that were used during data acquisition are summarized in Table 2. Data processing was the same across all transects (Ryan, 2011) and data made publically available from the IMOS-BASOOP repository (https://imos.aodn.org.au/imos123/). The minimum acquisition threshold was set at -120 decibels (dB) and the echo-integration cell was fixed at 10 m deep by 1 km long . A full metadata record was included with each transect following the International Council for the Exploration of the Sea (ICES) metadata convention (ICES, 2014).

2.2. MyctO-3D-MAP acoustic data collection and processing

Six summer and winter transects from four acoustic surveys were realized between February 2013 and August 2014 on board the R/V *Marion Dufresne II* (Table 1, Fig. 1). *In situ* acoustic data were recorded continuously (both day and night) using a Simrad EK60 split-beam echosounder at 38 and 120 kHz. Only the 38 kHz was analyzed in the present work. The

depth of the hull-mounted acoustic transducer was 6 m below the surface. As for the IMOS-BASOOP dataset, the acoustic MyctO-3D-MAP data were processed with an offset of 10 m below the sea surface. The echosounder systems were calibrated following the procedures recommended in Foote et al. (1987) before its installation onboard in 2012 and it was checked in 2014 and 2015. Data were recorded in *HAC* format (McQuinn et al., 2005) using ER60 software (Simrad, 2008). Data acquisition settings at 38 kHz were similar to those used during the IMOS-BASOOP cruises (Table 2).

Data processing was the same across all transects. Firstly, the Movies+ software (Ifremer development) was used for visually assessing the quality of the data prior to further analyses. Secondly, an in-house tool developed under Matlab (MATLAB 7.11.0.584, Release 2010b) in conjunction with the Movies3D software (Ifremer development) was used to filter the data, improve their quality and make them comparable to the IMOS-BASOOP data. This tool filters-out four types of noises: (i) ADCP interference, (ii) background noise, and both (iii) attenuated- and (iv) elevated-signals (Fig. 2). Echosounder and ADCP transmissions were synchronized, but residual ADCP interferences were detected on a ping-by-ping basis. Identified samples with interference were replaced by the means of the backscattering values one ping prior and one ping after the interference. Background noise was subtracted from the original data using a passive recording made every four hours during each survey. This allowed for an optimal estimation of the background noise that varies with weather conditions and ship speed. Attenuated- and elevated-signals are pings with substantially lower and higher backscattering values. To remove them, a sliding median (150 pings wide window) of backscattering values was calculated in two different continuous and homogenous layers for attenuated- and elevated-signals, respectively. For each ping, backscattering values in layers were compared to the sliding median values. If difference was over a predefined threshold (from +3 to +6 dB over median values for elevated signal and from -3 to -6 dB under median

values for attenuated signal, depending on data quality) the ping was removed. Finally, clean data was used for echo-integration by layer to quantify acoustic density of micronekton (Simmonds and MacLennan, 2005). The minimum acquisition and echo-integration thresholds were set at -120 and -80 dB, respectively. The echo-integration cell was fixed at 10 m deep by 1 km long in order to detect small-scale differences in acoustic responses across large-scale features (ICES, 2014).

2.3. Environmental data

Oceanographic data during the study periods were obtained from satellite measurements, namely (i) sea surface temperature (SST) gridded products at 9 km resolution obtained from the MODIS satellite (http://disc.sci.gsfc.nasa.gov/giovanni), and (ii) altimetric Absolute Dynamic Topography (ADT) gridded products at one-third degree resolution (AVISO, http://www.aviso.oceanobs.com). Average monthly maps corresponding to each transect were computed to avoid daily cloud interferences and because this temporal resolution is acceptable for studying large-scale features such as basin-scale frontal areas (Kostianoy et al., 2004). Isotherms and ADT contours together with SST and ADT gradients were taken as surface proxies of (sub-) surface fronts and used to delineate the main water masses of the South-Western Indian Ocean from 20 to 50°S. ADT gradients are useful to detect fronts within the Southern Ocean, while SST gradients are better indicators in the warmer Northern waters (Sokolov and Rintoul, 2002; Graham et al., 2012). Steep ADT gradients (≥ 25 cm/100 km) consistently correspond to nearly constant values of ADT contours and are indicative of fronts in the Southern Ocean (Sokolov and Rintoul 2007, 2009). SST gradients steeper than 2°C/100 km and surface isotherms taken together allow for the identification, from the North to the South, of the following fronts (Anilkumar et al.,

2007): the Northern Subtropical Front (NSTF) at 21-22°C, the Agulhas return Front (AF) at 17-19°C, the Southern Subtropical Front (SSTF) at 11-17°C, the Subantarctic Front (SAF) at 9-11°C and the Polar Front (PF) at 4-5°C. Satellite SST has previously been used to study the dynamic of these fronts (Lutjeharms and Valentine, 1984; Kostianoy et al., 2004), which showed a Southward shift in summer. The fronts delineate six oceanic zones, namely from the North to the South: the tropical zone (North of the NSTF), and the North subtropical, South subtropical, subantarctic, polar frontal and Antarctic (South of the PF) zones (Fig. 3). The Antarctic zone here corresponds to the Northern part of the Permanently Open Ocean Zone (POOZ; Tréguer and Jacques, 1992). Each echo-integration cell from each acoustic survey was assigned to a given oceanic zone after extracting SST and ADT and their gradient for each transect.

2.4. Data post-processing and statistical analysis

Data from both MyctO-3D-MAP and IMOS-BASOOP datasets were pooled and analyzed together. Acoustic density of micronekton was estimated by calculating the Nautical Area Scattering Coefficient (NASC, S_A, $m^2 \cdot nmi^{-2}$; MacLennan et al., 2002). NASC can be used as a proxy of micronekton abundance, assuming that the composition of the scattering layers and the resulting scattering properties of micronekton are homogeneous over the entire sampling region (*e.g.* Simmonds and MacLennan, 2005; Lawson et al., 2008). NASC calculated from the 38 kHz acoustic frequency may be a good proxy of micronekton abundance (Bertrand et al., 1999; McClatchie and Dunford, 2003; Kloser et al., 2009). Diel vertical variation of micronekton was assessed by analyzing daylight and nighttime and acoustic data separately. The crepuscular period (45 minutes before and after sunrise and sunset) during which micronekton ascends and descends (Lebourges-Dhaussy et al., 2000;

Benoit-Bird et al., 2009) were excluded from the analyses. An initial analysis of the echograms indicated that, as recently described for the tropical Indian Ocean (Béhagle et al., 2014), organisms were vertically structured in three main layers over the whole latitudinal range (20-50°S). The water column was therefore split into three layers and a backscattering (NASC) tool was developed to characterize the Surface Layer (SL), Intermediate Layer (IL) and Deep Layer (DL; Fig. 4). The lower depth boundary of the SL corresponds to 95% of the backscatter from the surface (10 m) to a depth ≤ 200 m (200 m depth being the lower limit of the epipelagic component). In the same way, the upper limit of the DL corresponds to 5% of the backscatter from an arbitrary mesopelagic limit value of 500 m to the depth limit of 800 m of our 38 kHz analysis. Finally, IL corresponds to the part of the water column between SL and DL.

All statistical analyses were performed within the R environment (R Core Team, 2014). The vegan (Oksanen et al. 2013) and const.clust (Legendre, 2012) packages were used for multivariate analyses. The RgoogleMaps (Loecher and Ropkins, 2015) package was used for map backgrounds. First, horizontal spatial autocorrelation in the acoustic data (*i.e.* spatial dependence between successive observations recorded along transects) was assessed using a Mantel correlogram. Data were first transformed using the Chord distance that is well suited to data that are supposed to be dependent (Legendre and Legendre, 2012). Linear trends in the linear acoustic transects were removed using linear models to avoid interference in autocorrelation response. Second, non-hierarchical k-means clustering was used to explore spatial variation in vertical acoustic structure. Third, spatially constrained hierarchical clustering, *i.e*. in which spatial contiguity is forced on the members of each cluster, was used to obtain spatially homogeneous clusters. The spatially constrained clustering, based on a Ward's agglomerative method, created hierarchical groups that took into account the geographical position of objects. For both clustering approaches, an optimal and objective

number of groups was defined, using the Calinski criterion for k-means clustering and the Akaike Information Criterion (AIC) for constrained clustering (Legendre and Legendre, 2012). Finally, potential relationships between clusters from each clustering methods and the main oceanic (inter-frontal) zones (macroscale oceanography, see above) were investigated using a correlation test based on the Chi-square method.

3. Results

3.1. Horizontal acoustic distribution of micronekton

NASC values (10-800 m depth) were calculated for each echo-integration cell of each transect. The resulting NASC distribution showed both latitudinal and seasonal changes (Fig. 5). In both seasons, NASC values peaked (> 5 000 m^2 nm^{-2}) at mid-latitudes with lower values in the northernmost and southernmost waters. The mid-latitude abundance peak shifted towards the north in the wintertime (30-47°S and 27-43°S in summer and winter, respectively). Longitudinal differences were observed in the southern area. NASCs located over the Crozet and Kerguelen shelves were low compared to higher values reported in the open waters between the two shelves.

3.2. Vertical acoustic distribution of micronekton

Total (10-800 m depth) and layer-integrated NASC values showed daily and seasonal changes. In summer, integrated NASC value varied little with the day-night cycle (Fig. 6). In contrast, in winter, micronektonic abundance had a contrasted day-night cycle with the highest total NASC value occurring at night during that season. Regardless of the daily cycle

and season, the vertical structuring of micronekton always followed the same pattern, with increasing abundances from the SL down to the DL: SL (7-23% of the total NASC values) < IL (28-35%) < DL (47-61%) (Fig. 6). However, SL NASC values increased at night, with concomitant decreases in both IL and DL values. Two-sample t-tests performed on NASC values confirmed significant summer and winter day/night differences ($t = -4.89$, $p < 0.001$) in SL, but not in IL and DL ($t = 0.58$ and 0.79 respectively, $p > 0.05$ for both).

3.3. Vertical acoustic distribution of micronekton across latitudes

Spatial variation in the vertical acoustic structure of micronekton was first investigated using unconstrained k-means clustering for each transects. The Calinski criterion indicated three to five optimal numbers of clusters, depending on transects and the diel cycle. For example, four and three distinct clusters were found for the day and night, respectively, for the transects illustrated in Fig. 7a,. The clusters were geographically dispersed and their vertical NASC profiles were significantly different ($F > 2.61\ 10^{27}$, $F > 1.50\ 10^{31}$ for day and night respectively, $p < 0.001$). Likewise, for spatially constrained clustering, AIC indicated an optimal number of groups comprised between three and five, depending on transects and diel cycle (Table 3). A strong latitudinal (20-50°S) structuring of the clusters was illustrated by the analysis (Fig. 7b), with, again, the vertical NASC profiles of the clusters being significantly different ($F > 2.67\ 10^{29}$, $F > 6.23\ 10^{28}$ for day and night respectively, $p < 0.001$).

3.4. Vertical acoustic distribution of micronekton and macroscale oceanography

To investigate potential relationships between spatially-constrained clusters and the main oceanic (inter-frontal) zones, a correlation test was performed for each transect, taking

into account both seasonality and the diel cycle because micronekton undergo daily vertical migration (Fig. 4) and the position of oceanic fronts varies with seasons (Fig. 8a). For example the NSTF was located ~5° further North in the wintertime, while there was almost no seasonal change in the latitudinal position of the PF. All tests were highly significant (Table 3), showing that there was a strong link between the location of the constrained clusters and the independently identified main oceanic zones. The same test was then performed on k-means clusters to confirm the relationships observed between clusters obtained from acoustic data and the main oceanic zones; all tests were significant. In other words, the vertical acoustic structure of the micronekton varied according to macroscale oceanography, and this relationship holds whether clustering is spatially constrained or not.

Mean vertical backscattering (NASC) profiles for each oceanic zone (Fig. 8b) illustrate spatial (horizontal and vertical) and temporal (seasonal and daily) variations in micronektonic distribution. Overall, total NASC values (10-800 m) varied 14-fold, from 3 843 (SSTZ during the day in summer) to 284 m^2 nm^{-2} (AZ at night in summer), and, depending on depth, from 2 079 (DL in SSTZ during the day in winter) to 29 m^2 nm^{-2} (SL in AZ at night in summer) (Table 4). Several features were notable: (i) as already underlined (see *section 3.2.* above), in most cases the vertical structure of the micronekton followed the same pattern of increasing abundance with depth (SL < IL < DL) and there was an obvious diel cycle, with higher abundances in the SL at night than during the day; (ii) overall, total NASC values (10-800 m) peaked in the subtropics (*e.g.* SSTZ) and low abundances occurred consistently in the PFZ (lowest value in the AZ). Hence, the seasonal shift in the latitudinal position of all five fronts (Fig. 3) induced a Northern latitudinal shift of the peak in abundance from summer to winter (see *section 3.1.* above); (iii) the warmer the waters, the higher SL NASC values generally were, with the highest absolute and relative (38-51% of the total abundance) values occurring at night in the TZ and the lowest abundance at night in the AZ; (iv) the high overall

abundance in subtropical waters (NSTZ and SSTZ) were mainly due to high NASC values in the IL and DL that contrasted with low surface values (SL), especially during the day (2-11%); (v) in contrast to the three Northern zones, the IL and DL NASC values were almost similar further South in the SAZ, PFZ and AZ; (vi) no major seasonal trend was found in terms of vertical structure, except that both absolute and relative SL NASC values were very low in winter in the PFZ, including at night (5-10%) (Table 4, Fig. 8).

4. Discussion

The key finding of this study is the strong correlation between the horizontal and vertical distribution of acoustic backscatter and physical oceanography (water masses) in the South-Western Indian Ocean. The structuring effect of oceanographic features on marine organisms has long been recognized at various scales and using different methods (*e.g.* Chelton et al., 2011; Lévy et al., 2012; Commins et al., 2013). To the best of our knowledge, however, no previous acoustic transects were conducted over such a large spatial range (20-50°S, 50-80°E) encompassing five major oceanic fronts delineating six different water masses. The circumpolar annular structure of fronts and water masses around the Antarctic Continent within the Southern Hemisphere (Deacon, 1982; Comiso et al., 1993) suggests that the structuring effect of successive latitudinal water masses on micronekton can be generalized to the Southern Atlantic and Pacific Oceans. The hypothesis of a similar large-scale circumpolar pattern of acoustic micronekton abundance merits further investigation, and does not preclude significant variations at a more regional scale (*e.g.* higher Antarctic krill abundance reaching lower latitudes in the South-Western Atlantic Ocean than elsewhere; Atkinson et al., 2008).

4.1. Methodological considerations

Acoustic sampling of micronekton contains its own uncertainties and potential sources of bias. First, the offset below the hull precludes measuring NASC values in the first 10 m of water that effectively is considered a dead-zone in our analysis. However, trawling in the top few meters of the water column may result in important micronekton biomasses captures, especially at night (O'Driscoll et al., 2009). Second, the low 38 kHz frequency offers the advantages of depth-penetration and low backscattering from non-target organisms, but suffers the disadvantages of fish swimbladder resonance and the virtual exclusion of aquatic organisms without gas-filled swimbladder due to their low target strength (Davison et al., 2015). Third, while micronektonic organisms are diverse and include crustaceans, cephalopods and fish, acoustics do not allow direct taxonomic identification of individuals contributing to the acoustic backscatter. Consequently, converting NASC values to micronekton biomass was not performed in the present study because it requires knowledge of the taxonomic composition along with information about the acoustic properties of each detected species (Davison et al., 2015). Fourth, species-specific acoustic properties also limit the use of NASC as a proxy of micronektonic biomass, because species composition varies in time and space according to many variables, including depth, daily vertical migration and water masses. However, biases were minimized here by using 38 kHz, the most appropriate frequency for micronekton, together with the relevant threshold of -80 dB to avoid backscatter from plankton and other smaller organisms while keeping a good signal/noise ratio (Kloser et al., 2009; Davison et al., 2015). These limitations are not expected to hinder the main conclusions of this study, namely the horizontal and vertical structures of the micronekton over large spatial and temporal scales.

Echograms at 38 kHz showed that micronektonic organisms were structured in three main layers within the sampled depth (10-800 m). Basically, there were two main layers with high concentrations of backscatter: one between the surface (10 m) and 100-200 m and another in the 350-700 m range. Lower NASC values were observed between these dense layers. A similar vertical structure of micronekton abundance was recently described in the tropical Indian Ocean (Béhagle et al., 2014) and it also occurs in the Pacific Ocean (Escobar-Flores et al. 2013). For analytical purposes, and because depth limits of the layers varied in time and space (Fig. 4 and 8), limits of the three layers were assessed using the total backscatter from the surface (10 m) to a depth ≤ 200 m (limit of the epipelagic zone) and the total backscatter from an arbitrary mesopelagic limit value of 500 m to the depth limit of 800 m of our 38 kHz analysis. Consequently, in this work, the layer-integrated NASC values (Table 4) corresponded to the distribution of well-defined micronektonic layers.

Finally, oceanic fronts that limit water masses were delineated using a combination of SST and ADT fields. These satellite-derived data had a larger spatial resolution (~9 and 36 km, respectively) than acoustic data (~1 km) collected during the surveys. This resolution mismatch has no major negative consequence on the analyses, because our main goal was not to relate NASC distribution with the fronts themselves, but, instead, to investigate at a larger spatial scale the breaking zones from physical and acoustic data and to assess the correlation of these breaks between the two datasets.

4.2. Diel vertical distribution of micronekton

A relevant part of the acoustic responses detected during this study was attributed to micronekton that typically migrate from deeper layers (IL and DL) to epipelagic waters (SL) at night and return to mesopelagic layers during the day (Fig. 4 and 6). Consequently, SL

NASC values increased at night, with concomitant decreases in both IL and DL values, which is in agreement with the well-known diel vertical migration of most micronektonic organisms (*e.g.* Lebourges-Dhaussy et al., 2000; Benoit-Bird et al., 2009; Godø et al., 2009; Drazen et al., 2011). Diurnal changes were more pronounced within the SL than the IL and DL. These changes likely result from: (i) the vertical migration of some organisms while others are semi-migrants or non-migrants, and thus remain in deeper layers all day long (Watanabe et al., 1999, 2006), and (ii) the upward migration of some micronektonic species from depths beyond the range of the 38 kHz transducer (> 800 m). Indeed, total NASC values (10-800 m) were greater at night than during the day, especially in winter (Fig. 6), indicating an upward migration of deep-dwelling organisms at sunset, as already observed in the Atlantic and Pacific Oceans (Domokos, 2009; Godø et al., 2012; Escobar-Flores et al., 2013; Béhagle et al., 2014). Another consistent feature of the vertical micronekton distribution in the present work is that NASC values overall increased in the order SL < IL < DL regardless of the spatial and temporal scales. Higher relative abundance in DL compared to SL (Table 4, Fig. 6) is a general feature during daytime. Interestingly, contrasted results are observed at night, in relation to the small to wide vertical movements of the ensonified organisms (Domokos, 2009; Escobar-Flores et al., 2013; Béhagle et al., 2014).

4.4. Micronekton and macroscale oceanography

The combination of active acoustics with remote sensing underlines the defining effect of macroscale oceanography on the distribution and abundance of micronekton in the South-Western Indian Ocean. Oceanic fronts are known to concentrate marine organisms and their predators, including air-breathing vertebrates (van Franeker et al., 2002; Bost et al., 2009), but few investigations have focused on oceanic zones themselves. Our study allowed defining a

mean backscattering vertical profile of micronekton associated to each oceanic zone, from the warm tropics to the cold waters of the low Antarctic zone (Fig. 8). Hence, fronts constitute true biogeographical boundaries delimiting relatively homogenous oceanic zones likely corresponding to the habitat and ecological optimum of organisms living within (Pakhomov and McQuaid, 1996; Koubbi et al., 2011; Commins et al., 2014). A first main result of this study is the peak in total NASC values (10-800 m) in the subtropics (*e.g.* SSTZ) with lower abundances observed in the Northern TZ and Southern SAZ and PFZ, and the lowest value in the AZ (Table 4). Few comparable data are available in the scientific literature, but an acoustic transect from New Zealand to Antarctica clearly showed similar high total NASC values (0-1000 m) in the North and much lower backscatter in the AZ (O'Driscoll et al., 2011). Higher micronektonic standing stocks in the subtropics fit well with enhanced surface chlorophyll concentrations and primary production in the subtropical zone of the Southern Hemisphere, especially in the African sector (~20-70°E) where high value corresponds to the Antarctic circumpolar current and lower values are found further South (Moore and Abbott, 2000). It is in agreement with the overall positive correlation between mid-water organisms and phytoplankton, with the putative underlying factor being food availability (Domokos, 2009; Escobar-Flores et al., 2013; Irigoien et al., 2014). A second main result is that the vertical structure of both absolute (m^2 nm^{-2}) and relative (%) micronekton abundance varies with water masses (Table 4, Fig. 8). For example, the high overall abundance in subtropical waters were mainly due to high NASC values at greater depths (IL and DL) that contrasted with low surface values (SL), while tropical waters are characterized by the highest NASC values in the SL, especially at night. This latter finding is in agreement with the acoustic SL being the dominant layer at night in the Central Pacific and the Mozambique Channel, but previous studies did not extent beyond tropical waters (Domokos, 2009; Béhagle et al., 2014).

Unfortunately, the scarcity of acoustic transects for oceanic waters at large horizontal and vertical scale precludes further comparisons with similar investigations (Irigoien et al., 2014).

A third and last main result is that, despite very low absolute and relative wintertime SL backscatters in the PFZ, no major seasonal differences in relative SL, IL and DL NASC values were found. An increasing seasonality with increasing latitudes is an obvious physical and biological feature with seasonality being at its maximum in high-Arctic and high-Antarctic waters (*e.g.* Moore and Abbott, 2000). Lower SL micronektonic abundance in winter in the PFZ corresponds to the presumed deepening of mid-water fish (Lancraft et al., 1991; Kozlov et al., 1995) and is associated to low surface chlorophyll concentrations and primary production at that time (Moore and Abbott, 2000). Higher seasonal changes including very low biomasses in SL can be expected further south, but a recent work challenged this view with important biomasses occurring in the very top of SL in ice-covered waters in winter (Flores et al. 2014). Finally, the Northern shift in total NASC values (Fig. 5) is well-explained by the concomitant northern shift of oceanic fronts (Fig. 8; Kim and Orsi, 2014), and hence of water masses with their associated backscatter structure in winter in the Southern Indian Ocean.

The present study highlights the added value of using large databases assembled from pooling comparable and independent acoustic records collected from both research and fishing vessels. In this way, numerous regular transects realized over years and seasons can ne analyzed together. The approach provides unique opportunities to gather basic information about the poorly known micronekton worldwide, and is a first preliminary and necessary step to describe oceanic zones of relevant biological interest in terms of trophic ecology. Clearly, however, the acoustic methods described here have to be complemented in several ways, mainly during research cruises. First, the acoustic backscatter needs to be partitioned to taxa and species (Handegard et al., 2013). The use of split-beam echosounders at multiple

frequencies and the concomitant development of analytical frequency-differencing techniques will aid in partitioning the ensonified organisms in taxonomic groups (*e.g.* Madureira et al., 1993; Korneliussen and Ona, 2003). Second, combined acoustic/trawl surveys are needed to assess species community composition in these areas (selected "focal areas"; Handegard et al., 2013). More specifically, a frequency response library can be made by repeated trawl samplings on discrete and identifiable acoustic layers (Gauthier et al., 2014). Third, converting species backscatter to biomass is another key issue requiring the quantification of acoustic properties of the targeted organisms (Davison et al., 2015). Finally, remote sensing provides accurate horizontal oceanographic information, but the accuracy of oceanic feature detections would increase by complementing remote sensing with vertical sampling. In this way it would be possible to relate backscatter distribution at different depths with the physical and chemical properties (*e.g.* temperature, salinity, oxygen, fluorescence; Bertrand et al., 2010; Lezama-Ochoa et al., 2014) of the water column.

Acknowledgements

The authors whish thank two anonymous referees and A. Lebourges-Dhaussy for helpful comments on previous versions of the manuscript. Gratitude is extended to F. D'Ovidio for providing complementary funding. The present work was financially and logistically supported by the Agence Nationale de La Recherche (ANR MyctO-3D-MAP, Programme Blanc SVSE 7 2011, Y. Cherel), the Institut Polaire Français Paul Emile Victor, and the Terres Australes et Antarctiques Françaises.

References

Anilkumar, N., Pednekar, S.M., Sudhakar, M., 2007. Influence of ridges on hydrographic parameters in the Southwest Indian Ocean. Mar. Geophys. Res. 28, 191-199.

Atkinson, A., Siegel, V., Pakhomov, E.A., Rothery, P., Loeb, V., Ross, R.M., Quetin, L.B., Schmidt, K., Fretwell, P., Murphy, E.J., Tarling, G.A., Fleming, A.H., 2008. Oceanic circumpolar habitats of Antarctic krill. Mar. Ecol. Prog. Ser. 362, 1-23.

Atkinson, A., Siegel, V., Pakhomov, E.A., Jessopp, M.J., Loeb, V., 2009. A re-appraisial of the total biomass and annual production of Antarctic krill. Deep-Sea Res. I 56, 727-740.

Bedford, M. Melbourne-Thomas, J., Corney, S., Jarvis, T., Kelly, N., Constable, A., 2015. Prey-field use by a Southern Ocean top predator: enhanced understanding using integrated datasets. Mar. Ecol. Prog. Ser. 526, 169–181.

Béhagle, N., du Buisson, L., Josse, E., Lebourges-Dhaussy, A., Roudaut, G., Ménard, F., 2014. Mesoscale features and micronekton in the Mozambique Channel: an acoustic approach. Deep-Sea Res. II 100, 164-173.

Benoit-Bird, K.J., Au, W.W.L., Wisdom, D.W., 2009. Nocturnal light and lunar cycle effects on diel migration of micronekton. Limnol. Oceanogr. 54, 1789-1800.

Bertrand, A., Ballon, M., Chaigneau, A., 2010. Acoustic observation of living organisms reveals the upper limit of the oxygen minimum zone. PLoS ONE 5, e10330.

Bertrand, A., Le Borgne, R., Josse, E., 1999. Acoustic characterisation of micronekton distribution in French Polynesia. Mar. Ecol. Prog. Ser. 191, 127-140.

Bianchi, D., Stock, C., Galbraith, E.D., Sarmiento, J.L., 2013. Diel vertical migration: ecological controls and impacts on the biological pump in a one-dimensional ocean model. Global Biogeochem. Cycles 27, 478-491.

Bocher, P., Cherel, Y., Labat, J.P., Mayzaud, P., Razouls, S., Jouventin, P., 2001. Amphipod-based food web: *Themisto gaudichaudii* caught in nets and by seabirds in Kerguelen waters, southern Indian Ocean. Mar. Ecol. Prog. Ser. 223, 261-276.

Bost, C.A., Cotté, C., Bailleul, F., Cherel, Y., Charrassin, J.B., Guinet, C., Ainley, D.G., Weimerskirch, H., 2009. The importance of oceanographic fronts to marine birds and mammals of the southern oceans. J. Mar. Sys. 78, 363-376.

Catul, V., Gauns, M., Karuppasamy, P.K., 2011. A review on mesopelagic fishes belonging to family Myctophidae. Rev. Fish. Biol. Fisheries 21, 339-354.

Chelton, D., Schlax, M., Samelson, R., 2011. Global observations of non linear mesoscale eddies. Prog. Oceanogr. 91, 167–216.

Comiso, J.C., McClain, C.R., Sullivan, C.W., Ryan, J.P., Leonard, C.L., 1993. Coastal zone color scanner pigment concentrations in the Southern Ocean and relationships to geophysical surface features. J. Geophys. Res. 98(C2), 2419-2451.

Commins, M.L., Ansorge, I., Ryan, P.G., 2014. Multi-scale factors influencing seabird assemblages in the African sector of the Southern Ocean. Antarct. Sci. 26, 38-48.

Cooper, J, Brown, C.R., 1990. Ornithological research at the sub-Antarctic Prince Edward Islands: a review of achievements. S. Afr. J. Antarct. Res. 20, 40-57.

Davison, P.C., Koslow, J.A., Kloser, R.J., 2015. Acoustic biomass estimation of mesopelagic fish: backscattering from individuals, populations, and communities. ICES J. Mar. Sci., in press.

Deacon, G.E.R., 1982. Physical and biological zonation in the Southern Ocean. Deep-Sea Res. 29, 1-15.

Domokos, R., 2009. Environmental effects on forage and longline fishery performance for albacore (*Thunnus alalunga*) in the American Samoa Exclusive Economic Zone. Fish. Oceanogr. 18, 419-438.

Drazen, J.C., De Forest, L.G., Domokos, R., 2011. Micronekton abundance and biomass in Hawaiian waters as influenced by seamounts, eddies, and the moon. Deep-Sea Res. I 58, 557-566.

Escobar-Flores, P., O'Driscoll, R.L., Montgomery, J.C., 2013. Acoustic characterization of pelagic fish distribution across the South Pacific Ocean. Mar. Ecol. Prog. Ser. 490, 169-183.

FAO, 2010. The state of world fisheries and aquaculture. FAO, Rome, Italy.

Fielding, S., Watkins, J.L., Collins, M.A., Enderlein, P., Venables, H.J., 2012. Acoustic determination of the distribution of fish and krill across the Scotia Sea in spring 2006, summer 2008 and autumn 2009. Deep-Sea Res. II 59-60, 173-188.

Flores, H., Hunt, B.P.V., Kruse, S., Pakhomov, E.A., Siegel, V., van Franeker, J.A., Strass, V., Van de Putte, A.P., Meesters, E.H.W.G., Bathmann, U., 2014. Seasonnal changes in the vertical distribution and community structure of Antarctic macrozooplakton and micronekton. Deep-Sea Res. I. 84, 127-141.

Foote, K.G., Knudsen, H.P., Vestnes, G., MacLennan, D.N., Simmonds, E.J., 1987. Calibration of acoustic instruments for fish density estimation: a practical guide. ICES Coop. Res. Rep. 144, 1-69.

Gauthier, S., Oeffner J., O'Driscoll, R.L., 2014. Species composition and acoustic signatures of mesopelagic organisms in a subtropical convergence zone, the New Zealand Chatham Rise. Mar. Ecol. Prog. Ser. 503, 23-40.

Godø, O.R., Patel, R., Pedersen, G., 2009. Diel migration and swimbladder resonance of small fish: some implications for analyses of multifrequency echo data. ICES J. Mar. Sci. 66, 1143-1148.

Godø, O.R., Reiss, C., Siegel, V., Watkins, J.L., 2014. Commercial fishing vessels as research vessels in the Antarctic. Requirements and solutions exemplified with a new vessel. CCAMLR Sci. 21, 11-17.

Godø, O.R., Samuelsen, A., Macaulay, G.J., Patel, R., Hjøllo, S.S., Horne, J., Kaartvedt, S., Johannessen, J.A., 2012. Mesoscale eddies are oases for higher trophic marine life. PLoS ONE 7, e30161.

Graham, R.M., de Boer, A.M., Heywood, K.J., Chapman, M.R., Stevens, D.P., 2012. Southern Ocean fronts: controlled by wind or topography? J. Geophys. Res. 117, C08018.

Guinet, C., Cherel, Y., Ridoux, V., Jouventin, P., 1996. Consumption of marine resources by seabirds and seals in Crozet and Kerguelen waters: changes in relation to consumer biomass 1962-85. Antarct. Sci., 8, 23-30.

Handegard, N.O., du Buisson, L., Brehmer, P., Chalmers, S.J., De Robertis, A., Huse, G., Kloser, R., Macaulay, G., Maury, O., Ressler, P.H., Stenseth, N.C., Godø, O.R., 2013. Towards an acoustic-based coupled observation and modelling system for monitoring and predicting ecosystem dynamics of the open ocean. Fish Fish. 14, 605-615.

Hunt, B.P.V., Hosie, G.W., 2006. The seasonal succession of zooplankton in the Southern Ocean south of Australia, part II: the Sub-Antarctic to Polar Frontal Zones. Deep-Sea Res. I 53, 1203–1223.

ICES, 2014. A metadata convention for processed acoustic data from active acoustic systems, SISP 4-TG-AcMeta, ICES WGFAST Topic Group, TG-ACMeta. 40 pp.

Irigoien, X., Klevjer, T.A., Røstad, A., Martinez, U., Boyra, G., Acuna, J.L., Bode, A., Echevarria, F., Gonzalez-Gordillo, J.I., Hernandez-Leon, S., Agusti, S., Aksnes, D.L., Duarte, C.M., Kaartvedt, S., 2014. Large mesopelagic fishes biomass and trophic efficiency in the open ocean. Nature Comm. 5, 3271.

Kaartvedt, S., Staby, A., Aksnes, D.L., 2012. Efficient trawl avoidance by mesopelagic fishes causes large underestimation of their biomass. Mar. Ecol. Prog. Ser. 456, 1–6.

Karp, W.A., 2007. Collection of acoustic data from fishing vessels. ICES Coop. Res. Rep. 287, 1-84.

Kim, Y.S., Orsi, A.H., 2014. On the variability of Antarctic circumpolar current fronts inferred from 1992-2011 altimetry. J. Phys. Oceanogr. 44, 3054-3071.

Kloser, R.J., Ryan T.E., Young, J.W., Lewis, M.E., 2009. Acoustic observations of micronekton fish on the scale of an ocean basin: potential and challenges. ICES J. Mar. Sci. 66, 998-1006.

Koizumi, K., Hiratsuka, S., Saito, H. 2014. Lipid and fatty acids of three edible myctophids, *Diaphus watasei, Diaphus suborbitalis,* and *Benthosema pterotum*: high levels of icosapentaenoic and docosahexaenoic acids. J. Oleo Sci. 63, 461-470.

Korneliussen, R.J., Ona, E., 2003. Synthetic echograms generated from the relative frequency response. ICES J. Mar. Sci. 60, 636-640.

Kostianoy, A.G., Ginzburg, A.I., Frankignoulle, M., Delille, B., 2004. Fronts in the Southern Indian Ocean as inferred from satellite sea surface temperature data. J. Mar. Sys. 45, 55-73.

Koubbi, P., Moteki, M., Duhamel, G., Goarant, A., Hulley, P.A., O'Driscoll, R., Ishimaru, T., Pruvost, P., Tavernier, E., Hosie, G., 2011. Ecoregionalisation of myctophid fish in the Indian sector of the Southern Ocean: results from generalized dissimilarity models. Deep-Sea Res. II 58, 170-180.

Kozlov, A.N., 1995. A review of the trophic role of mesopelagic fish of the Family Myctophidae in the Southern Ocean ecosystem. CCAMLR Sci. 2, 71-77.

Lancraft, T.M., Hopkins, T.L., Torres, J.J., Donnelly, J., 1991. Oceanic micronektonic/macrozooplanktonic community structure and feeding in ice covered Antarctic waters during the winter (AMERIEZ 1988). Polar Biol. 11, 157-167.

Lawson, G.L., Wiebe, P.H., Stanton, T.K., Ashjian, C.J., 2008. Euphausiid distribution along the Western Antarctic Peninsula. Part A: development of robust multi-frequency acoustic techniques to identify euphausiid aggregations and quantify euphausiid size, abundance, and biomass. Deep-Sea Res. II 55, 412-431.

Lebourges-Dhaussy, A., Marchal, E., Menkès, C., Champalbert, G., Biessy, B., 2000. *Vinciguerria nimbaria* (micronekton), environment and tuna: their relationships in the Eastern Tropical Atlantic. Oceanol. Acta 23, 515–528.

Legendre, P., 2012. Space-constrained or time-constrained agglomerative clustering from a dissimilarity matrix computed from multivariate data. http://adn.biol.umontreal.ca/~numericalecology/Rcode/

Legendre, P., Legendre, L., 2012. Numerical ecology. 3rd English edition. Elsevier, Amsterdam, The Netherlands.

Lévy, M., Ferrari, R., Franks, P.J.S., Martin, A.P., Rivière, P., 2012. Bringing physics to life at the submesoscale. Geophys. Res. Lett. 39, 1–13.

Lezama-Ochoa, A., Irigoien, X., Chaigneau, A., Quiroz, Z., Lebourges-Dhaussy, A., Bertrand, A., 2014. Acoustics reveals the presence of a macrozooplankton biocline in the Bay of Biscay in response to hydrological conditions and predator-prey relationships. PLoS ONE 9, e88054.

Loecher, M., Ropkins, K., 2015. RgoogleMaps and loa: unleashing R graphics power on map tiles. J. Stat. Softw. 63, 1–18.

Lutjeharms, J.R.E., Valentine, H.R., 1984. Southern Ocean thermal fronts south of Africa. Deep-Sea Res. 31, 1461-1475.

MacLennan, D.N., Fernandes, P.G., Dalen, J. 2002. A consistent approach to definitions and symbols in fisheries acoustics. ICES J. Mar. Sci. 59, 365-369.

MacLennan, D.N., Simmonds, E.J., 1992. Fisheries acoustics. First ed., Chapman and Hall, London, UK.

Madureira, L.S.P., Everson, I., Murphy, E.J., 1993. Interpretation of acoustic data at two frequencies to discriminate between Antarctic krill (*Euphausia superba* Dana) and other scatterers. J. Plankton Res. 15, 787-802.

McClatchie, S., Dunford, A., 2003. Estimated biomass of vertically migrating mesopelagic fish off New Zealand. Deep-Sea Res. I 50, 1263–1281.

McQuinn, I.H., Reid, D., Berger, L., Diner N., Heatley, D., Higginbottom, I., Andersen, L.N., Langeland, O., Lapierre, J.P., 2005. Description of the ICES *HAC* standard data exchange format, version 1.60. ICES Coop. Res. Rep. 278, 1-84.

MATLAB 7.11.0.584, Release 2010b, The MathWorks, Inc., Natick, Massachusetts, United States.

Menon, N.G., 2004. Potential exploitable micronektons from the Deep Scattering Layers (DSL) of the Indian EEZ. Mar. Fish. Infor. Serv. T&E Ser. 182, 1-9.

Miller, D.G.M., 1982. Results of a combined hydroacoustic and midwater trawling survey of the Prince Edward Island group. S. Afr. J. Antarct. Res. 12, 3-22.

Moore, J.K., Abbott, M.R., 2000. Phytoplankton chlorophyll distributions and primary production in the Southern Ocean. J. Geophys. Res. 105(C12), 28,709-28,722.

Nicol, S., Foster, J., Kawaguchi, S., 2012. The fishery for Antarctic krill, recent developments. Fish Fish. 13, 30-40.

O'Driscoll, R.L., Gauthier, S., Devine, J.A., 2011. Acoustic estimates of mesopelagic fish : as clear as day and night? ICES J. Mar. Sci. 66, 1310-1317.

O'Driscoll, R.L., Macaulay G.J., Gauthier, S., Pinkerton, M., Hanchet, S., 2011. Distribution, abundance and acoustic properties of Antarctic silverfish (*Pleuragramma antarcticum*) in the Ross Sea. Deep-Sea Res. II 58, 181-195.

Oksanen, J., Blanchet, F.G., Kindt, R., Legendre, P., Minchin, P.R., O'Hara, R.B., Simpson, G.L., Solymos, P., Stevens, M.H.H., Wagner, H., 2013. Community Ecology Package. https://github.com/vegandevs/vegan

Pakhomov, E., McQuaid, C.D., 1996. Distribution of surface zooplankton and seabirds across the Southern Ocean. Polar Biol. 16, 271-286.

Pakhomov, E.A., Froneman, P.W., 1999. Macroplankton/micronekton dynamics in the vicinity of the Prince Edward Islands (Southern Ocean). Mar. Biol. 134, 501-515

Pakhomov, E., Yamamura, O., 2010. Report of the advisory panel on micronekton sampling inter-calibration experiment. PICES Scient. Rep. 38, 1-108.

Park, Y.H., Gamberoni, L., 1995. Large-scale circulation and its variability in the south Indian Ocean from TOPEX/POSEIDON altimetry. J. Geophys. Res. 100 (C12), 24911–24929.

Perissinotto, R., McQuaid, C.D., 1992. Land-based predator impact on vertically migrating zooplankton and micronekton advected to a Southern Ocean archipelago. Mar. Ecol. Prog. Ser. 80, 15-27.

Pollard, R.T., Read, J.F., 2001. Circulation pathways and transports of the Southern Ocean in the vicinity of the Southwest Indian Ridge. J. Geophys. Res. 106 (C2), 2881– 2898.

Potier, M., Marsac, F., Cherel, Y., Lucas, V., Sabatié, R., Maury, O., Ménard, F., 2007. Forage fauna in the diet of three large pelagic fishes (lancetfish, swordfish and yellowfin tuna) in the western equatorial Indian Ocean. Fish. Res. 83, 60-72.

R Core Team, 2014. R: a language and environment for statistical computing. R Foundation for Statistical Computing, Vienna, Austria. URL http://www.R-project.org/.

Robertson, K.M., Chivers, S.J., 1997. Prey occurrence in pantropical spotted dolphins, *Stenella attenuata*, from the eastern tropical Pacific. Fish. Bull., 95, 334-348.

Rodhouse, P.G., Nigmatullin, C.M., 1996. Role as consumers. Phil. Trans. R. Soc. Lond. 351, 1003-1022.

Ryan, T., 2011. Overview of data collection, management and processing procedures of underway acoustic data. IMOS BASOOP sub-facility. http://imos.org.au/fileadmin/user_upload/shared/SOOP/plugin-IMOS_data_collection_and_processing_v1.01.pdf

Sabarros, P.S., Ménard, F., Lévénez, J.J., Tew-Kai, E., Ternon, J.F., 2009. Mesoscale eddies influence distribution and aggregation patterns of micronekton in the Mozambique Channel. Mar. Ecol. Prog. Ser. 395, 101–107.

Shaviklo, A.R., Rafipour, F., 2013. Surimi and surimi seafood from whole ungutted myctophid mince. LWT-Food Sci. Technol. 54, 463–468.

Simmonds, E.J., MacLennan, D.N., 2005. Fisheries acoustics: theory and practice. Second ed., Wiley-Blackwell, Oxford, UK.

Simrad, 2008. Simrad ER60, scientific echo sounder, reference manual. Technology for sustainable fisheries, Simrad, Kongsberg, Norway.

Sokolov, S., Rintoul, S.R., 2002. Structure of Southern Ocean fronts at 140°E. J. Mar. Syst. 37, 151-184.

Sokolov, S., Rintoul, S.R., 2007. On the relationship between fronts of the Antarctic Circumpolar Current and surface chlorophyll concentrations in the Southern Ocean. J. Geophys. Res. 112, C07030.

Sokolov, S., Rintoul, S.R., 2009. Circumpolar structure and distribution of the Antarctic Circumpolar Current fronts: 1. Mean circumpolar paths. J. Geophys. Res. 114, C11018.

Spear, L.B., Ainley, D.G., Walker, W.A., 2007. Foraging dynamics of seabirds in the eastern tropical Pacific Ocean. Studies Avian Biol. 35, 1-99.

Stramma, L., Lutjeharms, J.R.E., 1997. The flow field of the subtropical gyre of the South Indian Ocean. J. Geophys. Res. 102 (C3), 5513–5530.

Tréguer, P., Jacques, G., 1992. Dynamics of nutrients and phytoplankton, and fluxes of carbon, nitrogen and silicon in the Antarctic Ocean. Polar Biol. 12, 149-162.

van Franeker, J.A., van den Brink, N.W., Bathmann, U.V., Pollard, R.T., de Baar, H.J.W., Wolff, W.J., 2002. Responses of seabirds, in particular prions (*Pachyptila* sp.), to small-scale processes in the Antarctic Polar Front. Deep-Sea Res. II 49, 3931-3950.

Watanabe, H., Kubodera, T., Moku, M., Kawaguchi, K., 2006. Diel vertical migration of squid in the warm core ring and cold water masses in the transition region of the western North Pacific. Mar. Ecol. Prog. Ser. 315, 187-197

Watanabe, H., Moku, M., Kawaguchi, K., Ishimaru, K., Ohno, A., 1999. Diel vertical migration of myctophid fishes (Family Myctophidae) in the transitional waters of the western North Pacific. Fish. Oceanogr. 8, 115-127.

Woehler, E.J., Green, K., 1992. Consumption of marine resources by seabirds and seals at Heard Island and the McDonald Islands. Polar Biol.12, 659-665.

Table 1

Details of IMOS and MyctO-3D-MAP acoustic transects, including cruise names, seasons (summer or winter), starting and ending locations (latitude, longitude), starting and ending times (date, time GMT) and the run distances (km).

Database	Cruise	Season	Starting location	Starting time	End location	Ending time	Distance (km)
IMOS-BASOOP	SC012010	Summer	51.31°S, 71.57°E	01/19/2010 15:14	40.66°S, 45.98°E	01/24/2010 09:13	2 019
	SC032010	Summer	36.52°S, 52.15°E	02/27/2010 02:25	20.27°S, 57.21°E	03/03/2010 03:15	1 652
	SC032011	Summer	23.59°S, 58.09°E	03/16/2011 08:41	45.26°S, 66.31°E	03/21/2011 13:29	2 143
	AL072011	Winter	26.39°S, 60.38°E	07/07/2011 07:21	45.21°S, 69.00°E	07/12/2011 06:16	1 935
	WW082011	Winter	21.23°S, 56.96°E	07/30/2011 16:01	37.39°S, 50.59°E	08/03/2011 21:27	1 609
	AL092011	Winter	42.64°S, 78.06°E	09/04/2011 00:31	20.61°S, 57.40°E	09/11/2011 20:39	2 998
	AL052012	Summer	20.15°S, 57.49°E	04/29/2012 08:09	47.17°S, 66.24°E	05/06/2012 01:37	2 740
	AL072012	Winter	49.88°S, 77.20°E	07/23/2012 10:36	20.38°S, 57.27°E	07/31/2012 10:23	3 346
	AL082012	Winter	22.84°S, 58.37°E	08/09/2012 06:17	50.53°S, 75.29°E	08/17/2012 07:46	3 002
	SC112012	Summer	52.13°S, 74.79°E	11/07/2012 20:04	20.68°S, 57.30°E	11/16/2012 21:24	3 229
	AL122012	Summer	22.67°S, 58.19°E	12/15/2012 02:16	51.34°S, 77.20°E	12/22/2012 19:07	3 267
	AL022013	Summer	50.32°S, 77.68°E	02/04/2013 03:57	20.83°S, 57.42°E	02/13/2013 08:43	3 350
MyctO-3D-MAP	LOGIPEV193_RUNKER	Summer	30.12°S, 54.44°E	02/09/2013 06:07	49.17°S, 66.95°E	02/17/2013 17:48	2 752
	LOGIPEV193_KERMAU	Summer	46.96°S, 72.04°E	02/26/2013 04:24	22.62°S, 57.57°E	03/10/2013 23:26	2 012
	OP2013-2_RUNKER	Winter	21.18°S, 55.13°E	08/30/2013 07:48	49.95°S, 60.68°E	09/10/2013 22:48	3 310
	LOGIPEV197_RUNKER	Summer	21.56°S, 55.09°E	01/06/2014 21:15	49.16°S, 66.98°E	01/17/2014 22:43	2 596

LOGIPEV197_KERMAU	Summer	47.20°S, 71.95°E	02/06/2014 03:55	20.54°S, 57.26°E	02/18/2014 00:21	2 045
OP2014-2_RUNKER	Winter	15.99°S, 54.51°E	08/24/2014 10:10	49.47°S, 67.27°E	09/04/2014 06:47	3 677

Table 2

Simrad EK60 and ES60 echo sounder parameter settings onboard four different vessels.

Setting 38 kHz	Vessels			
	RV *Marion Dufresne II*	FV *Austral Leader II*	FV *Southern Champion*	FV *Will Watch*
Transducer type	ES38-B	ES38-B	ES38-B	ES38-B
Transducer depth (m)	6	7	7	6
Max. power (W)	1000	2000	2000	2000
Pulse duration (ms)	1.024	2.048	1.024	2.048
Ping interval (s)	1.5	2	2	2
Target Strenght (TS) gain (dB)	24.65	24.9	25.27	26.22
Area backscattering coefficient (Sa) correction	-0.03	-0.49	-0.65	-1.124
Sample length (m)	0.195	0.384	0.195	0.384

Table 3

Results of the Chi-squared tests showing the relationship between spatially-constrained clusters (vertical structure of the micronekton abundance) and the main oceanic zones (macroscale oceanography) for each transect and during the diel cycle. All p-values were lower than 0.001.

		Day		Night	
Database	Cruise	Optimal number of cluster	χ^2	Optimal number of cluster	χ^2
IMOS-BASOOP	SC012010	4	928	5	1660
	SC032010	4	887	3	124
	SC032011	3	1917	3	1049
	AL072011	5	1056	4	2053
	WW082011	5	1292	4	1926
	AL092011	3	2936	3	2981
	AL052012	3	1013	5	3577
	AL072012	5	3275	5	5056
	AL082012	5	4200	5	5297
	SC112012	3	695	3	2255
	AL122012	3	1865	5	6206
	AL022013	3	1443	5	3204
MyctO-3D-MAP	LOGIPEV193_RUNKER	4	2764	5	2796
	LOGIPEV193_KERMAU	5	699	5	1195
	OP2013-2_RUNKER	5	4075	4	5940
	LOGIPEV197_RUNKER	3	2738	4	2782
	LOGIPEV197_KERMAU	5	1826	4	1760
	OP2014-2_RUNKER	5	5764	4	5625

Table 4

Mean NASC values (m^2 nmi^{-2}) in the water column (10-800 m) according to (i) oceanographic zones, (ii) depth layers, (iii) seasons and (iv) the diel cycle. Values are means ± SD with n in parentheses.

Oceanic zones		Summer		Winter	
		Day	Night	Day	Night
Tropical (TZ)	Surface layer	(11) 249±116	(11) 827±324	(6) 273±113	(6) 925±181
	Intermediate layer	(11) 351±118	(11) 545±370	(6) 335±186	(6) 356±215
	Deep layer	(11) 986±373	(11) 817±342	(6) 861±222	(6) 531±210
	Total	**1586**	**2189**	**1469**	**1812**
North Subtropical (NSTZ)	Surface layer	(11) 214±122	(11) 403±160	(6) 250±117	(7) 575±256
	Intermediate layer	(11) 1172±745	(11) 967±428	(6) 344±215	(7) 317±278
	Deep layer	(11) 1822±820	(11) 1577±858	(6) 1635±438	(7) 1232±365
	Total	**3209**	**2947**	**2229**	**2124**
South Subtropical (SSTZ)	Surface layer	(7) 126±116	(8) 286±194	(6) 68±73	(7) 310±193
	Intermediate layer	(7) 1680±1545	(8) 948±593	(6) 1119±490	(7) 853±524
	Deep layer	(7) 2037±995	(8) 1281±534	(6) 2079±569	(7) 1817±693
	Total	**3843**	**2514**	**3266**	**2980**
Subantarctic (SAZ)	Surface layer	(5) 83±118	(6) 271±65	(4) 139±243	(5) 139±48
	Intermediate layer	(5) 943±787	(6) 771±404	(4) 1006±665	(5) 935±611
	Deep layer	(5) 950±911	(6) 831±534	(4) 1063±628	(5) 996±646
	Total	**1976**	**1873**	**2208**	**2070**
Polar Frontal (PFZ)	Surface layer	(9) 104±57	(7) 170±88	(4) 46±16	(4) 97±45
	Intermediate layer	(9) 464±124	(7) 333±85	(4) 396±212	(4) 437±160
	Deep layer	(9) 662±357	(7) 414±278	(4) 535±499	(4) 483±228
	Total	**1230**	**918**	**976**	**1016**
Antarctic (AZ)	Surface layer	-	(3) 29±16	-	-
	Intermediate layer	-	(3) 135±35	-	-
	Deep layer	-	(3) 120±43	-	-
	Total	**-**	**284**	**-**	**-**

Fig. 1. Map of survey area showing acoustic transects from the IMOS-BASOOP (blue) and MyctO-3D-MAP (red) databases, in summer (left) and winter (right).

Fig. 2. None filtered (upper panel) and filtered (lower panel) echograms illustrating the filtering tool that was developed in this work. The two echograms correspond to the same part of the OP2014-2_RUNKER transect with a horizontal shift on the filtered panel causes by the removing of bad data.

Fig. 3. Macroscale oceanographic maps of the study area in summer (left) and winter (right). Fronts were characterized from satellite data (sea surface temperature and altimetry, see text) to define the main oceanic (inter-frontal) zones of the South-Western Indian Ocean.

Fig. 4. Summer (upper panel) and winter (lower panel) echograms illustrating vertical micronektonic abundance distribution during one complete day-night cycle. The figure shows (i) the diel migration of micronekton during the transition period (blanked spaces), (ii) the three main depth layers (in solid red lines) that structure vertically the micronektonic abundance in the South-Western Indian Ocean, and (iii) the in-house tool limits used to define these main depth layers (in dashed red lines). Abbreviations: DL, deep layer, IL, intermediate layer, SL, surface layer.

Fig. 5. Latitudinal and NASC values (in m^2 nmi^{-2}) integrated from 10 to 800 m depth (a proxy of the overall micronektonic abundance distribution) during the 18 IMOS-BASOOP and MyctO-3D-MAP summer and winter transects.

Fig. 6. Overall temporal (diel and seasonal) changes of total (10-800 m) and layer-integrated NASC values (in m^2 nmi^{-2}) during the 18 IMOS-BASOOP and MyctO-3D-MAP summer and winter transects.

Fig. 7. Example of mean NASC profiles (in m^2 nmi^{-2}) of micronekton abundance across latitudes according to both k-means (a) and spatially-constrained hierarchical (b) clustering methods for the OP2013-2_RUNKER transect.

Fig. 8. (a) Average latitudinal position of oceanic fronts during the IMOS-BASOOP and MyctO-3D-MAP transects; the fronts delimit the main oceanic zones crossed during transects. (b) Mean NASC scaled profiles (in m^2 nmi^{-2}) of micronekton abundance according to (i) oceanic zones, (ii) seasons (summer and winter) and (iii) the diel cycle (day and night).

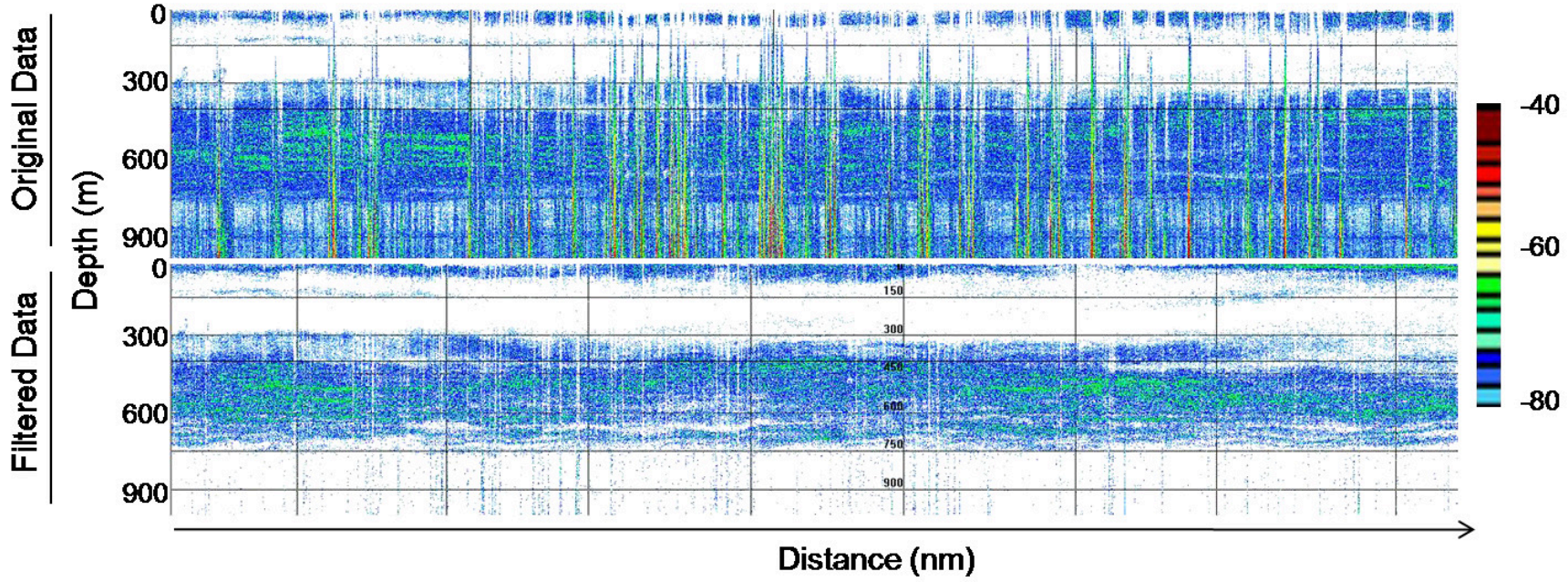
Original Data
Filtered Data
Depth (m)
0
300
600
900
0
300
600
900
150
300
450
600
750
900
-40
-60
-80
Distance (nm)

Figure 2

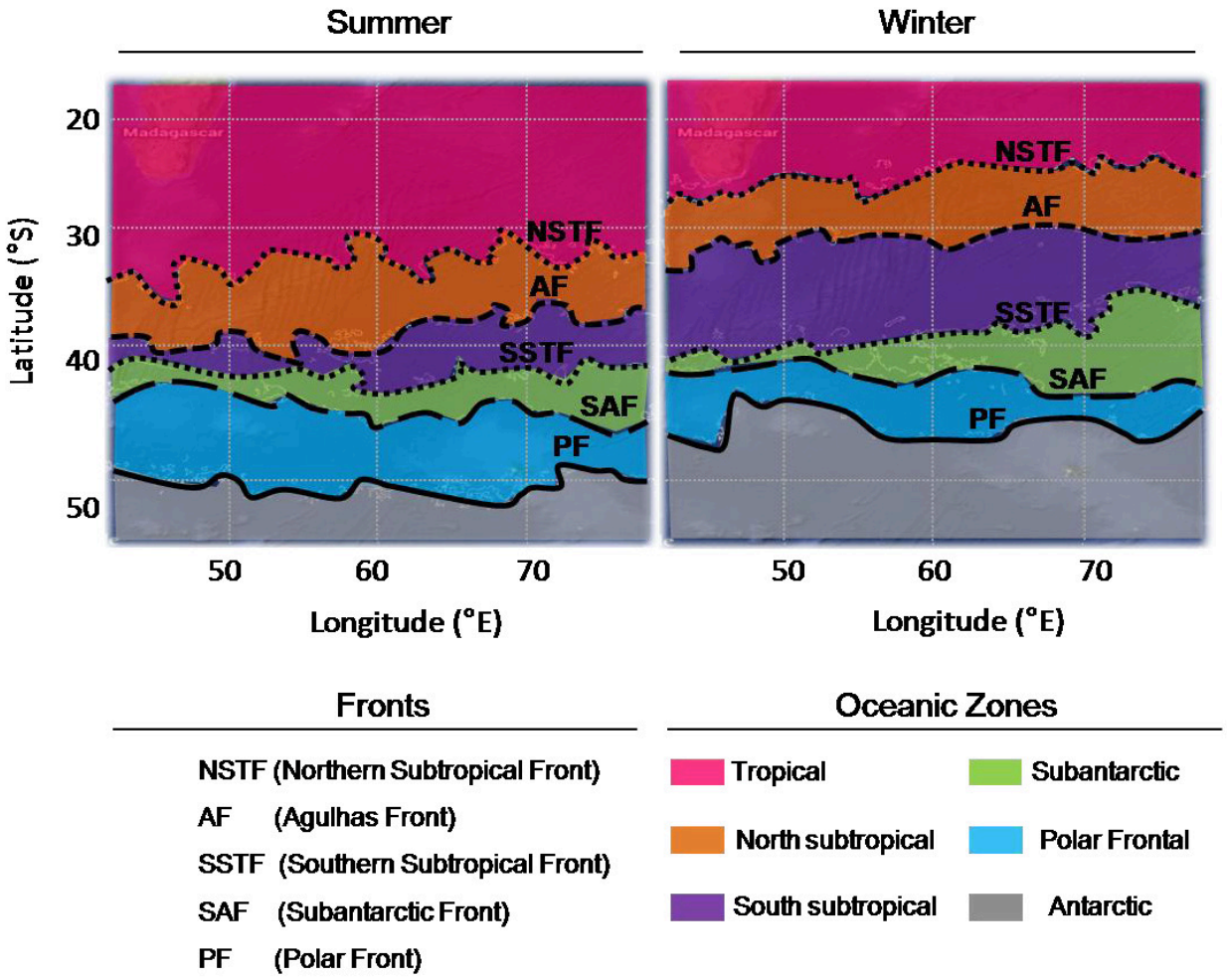
Summer
Winter
Latitude (°S)
20
30
40
50
50
60
70
Longitude (°E)
Madagascar
NSTF
AF
SSTF
SAF
PF
Fronts
NSTF (Northern Subtropical Front)
AF (Agulhas Front)
SSTF (Southern Subtropical Front)
SAF (Subantarctic Front)
PF (Polar Front)
Oceanic Zones
Tropical
Subantarctic
North subtropical
Polar Frontal
South subtropical
Antarctic

Figure 3

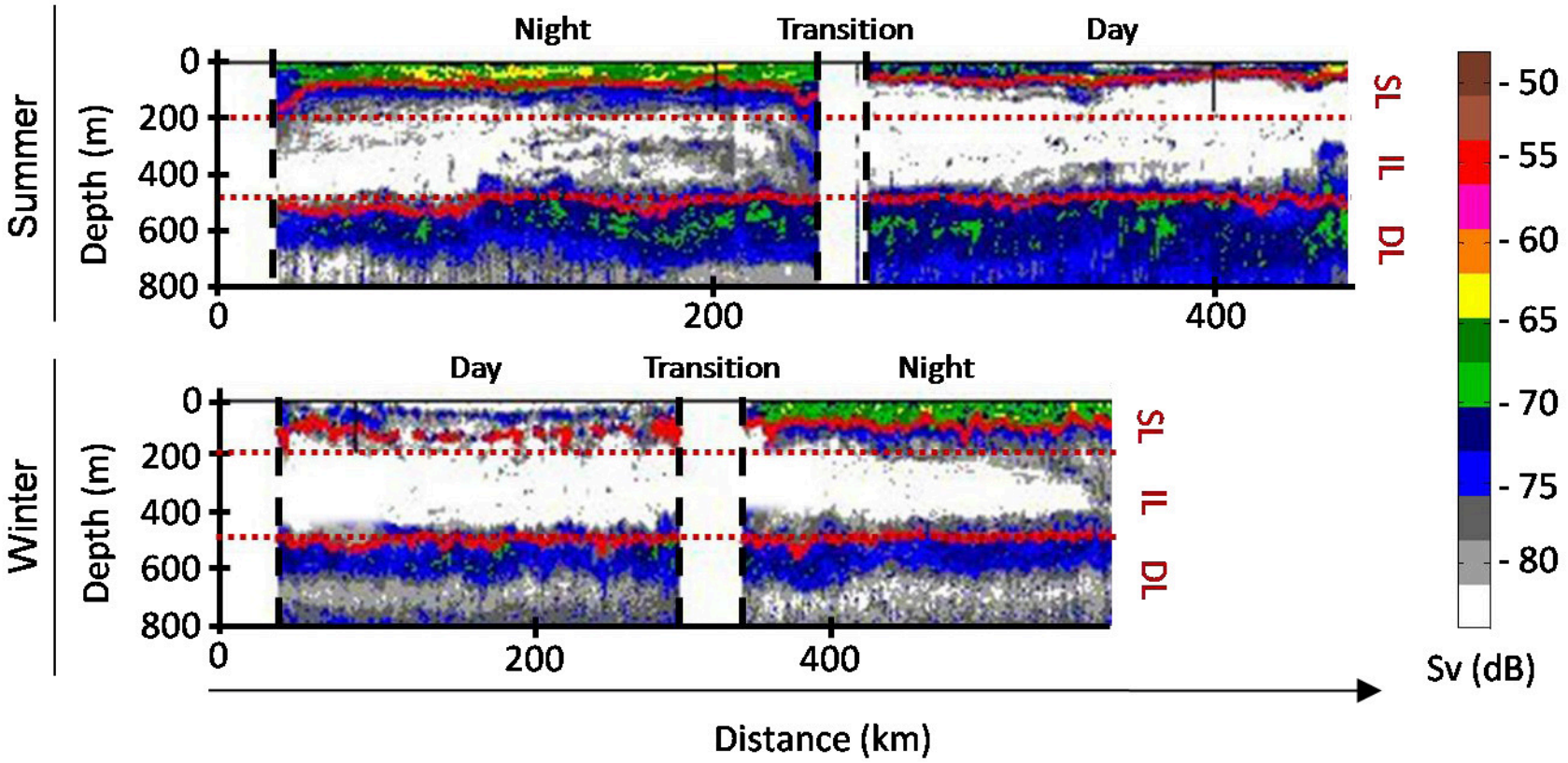
Summer
Depth (m)
Night
Transition
Day
0
200
400
600
800
0
200
400
SL
IL
DL
Winter
Depth (m)
Day
Transition
Night
0
200
400
600
800
0
200
400
SL
IL
DL
Distance (km)
50
55
60
65
70
75
80
Sv (dB)

Figure 4

800

801

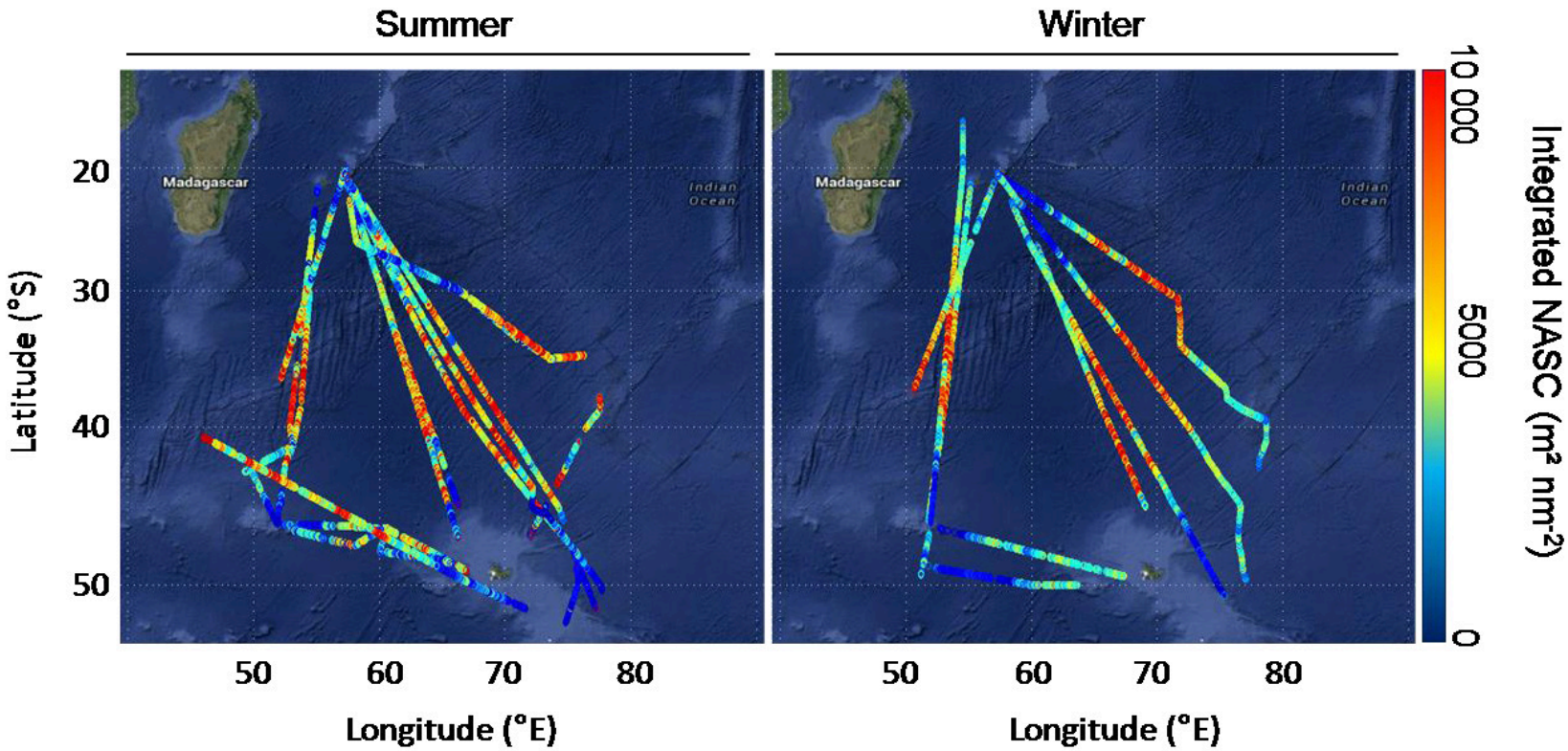

802

803

804 Figure 5

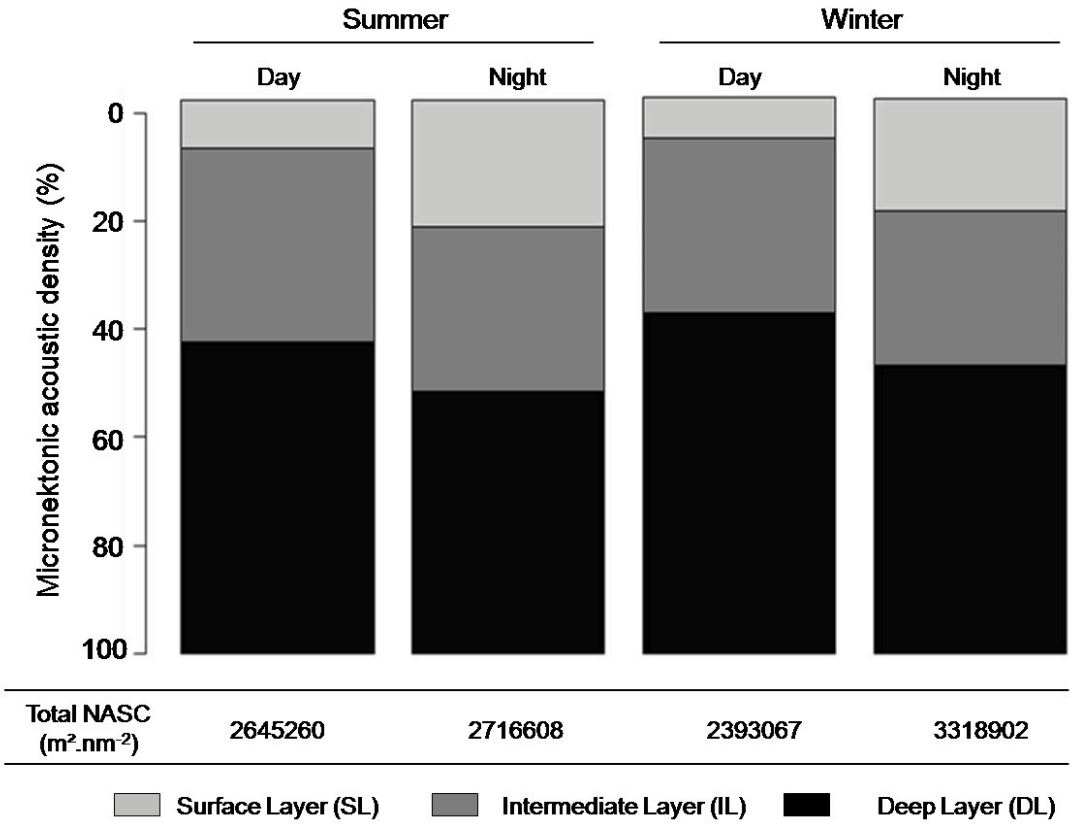
Summer
Winter
Day
Night
Day
Night
0
20
40
60
80
100
Micronektonic acoustic density (%)
Total NASC (m².nm⁻²)
2645260
2716608
2393067
3318902
Surface Layer (SL)
Intermediate Layer (IL)
Deep Layer (DL)

Figure 6

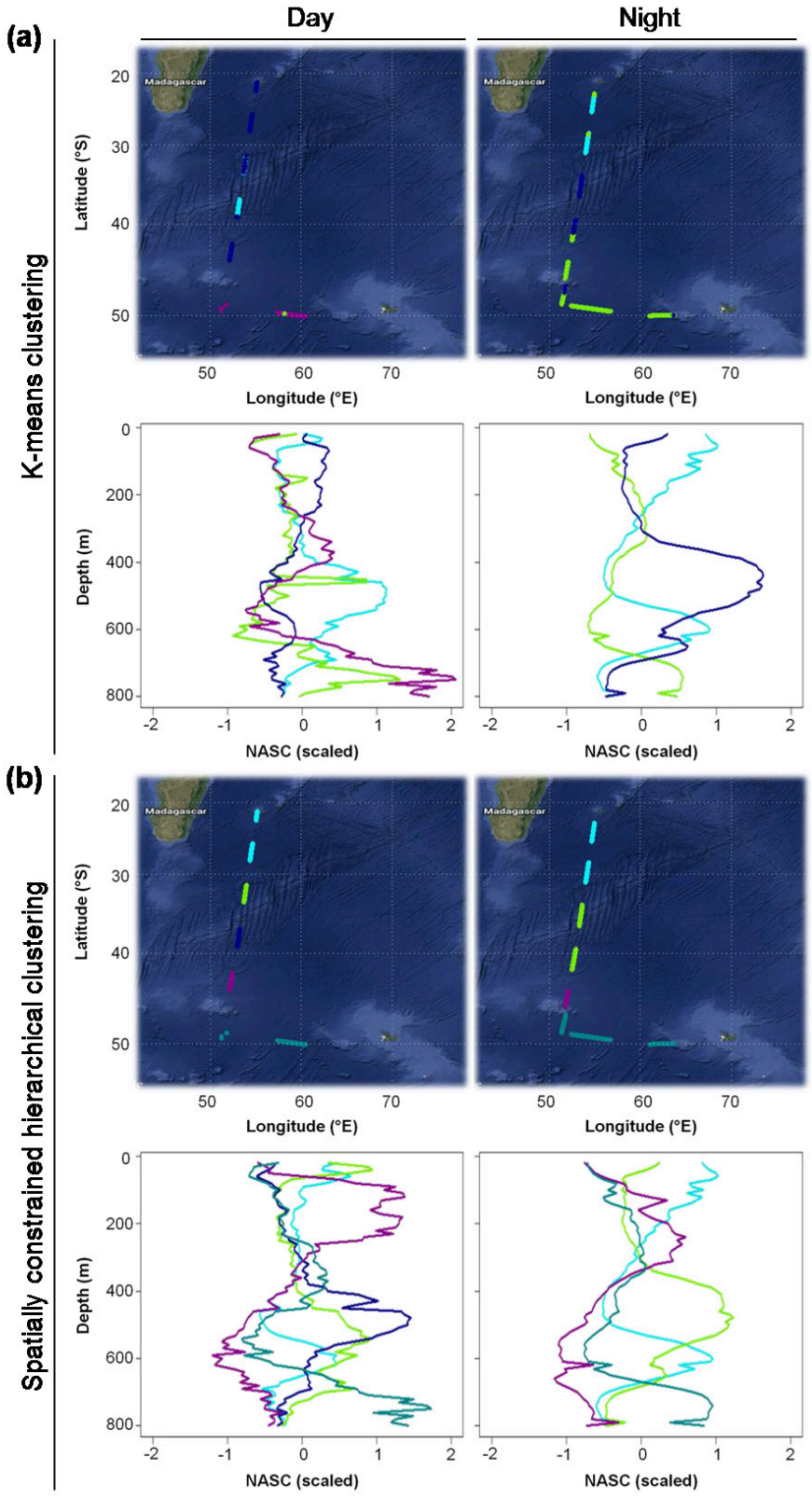
(a)
K-means clustering
Day
Night
Madagascar
Latitude (°S)
Longitude (°E)
Depth (m)
NASC (scaled)
(b)
Spatially constrained hierarchical clustering

Figure 7

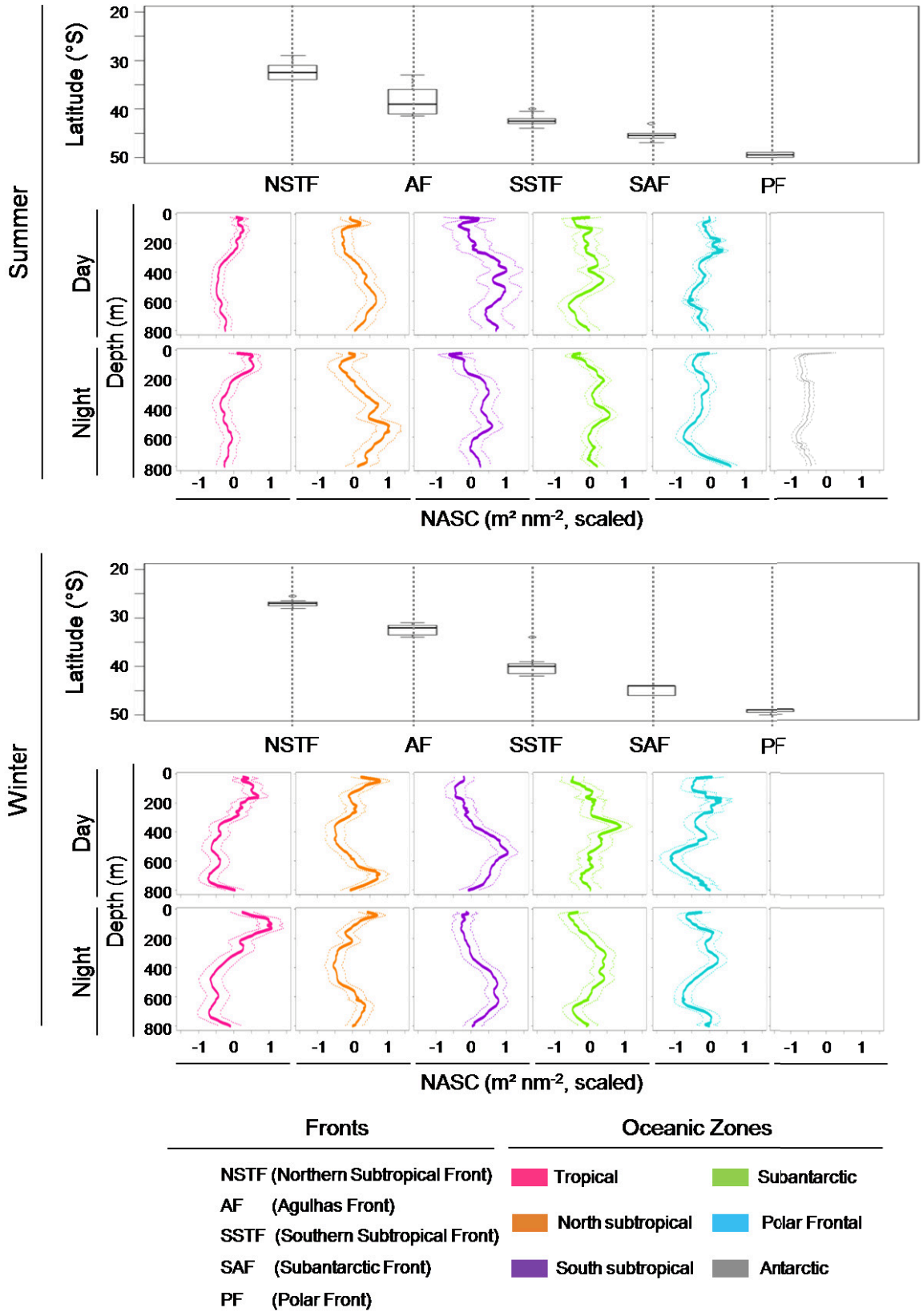
Summer
Latitude (°S)
20
30
40
50
NSTF
AF
SSTF
SAF
PF
Day
Night
Depth (m)
0
200
400
600
800
-1
0
1
NASC (m² nm⁻², scaled)
Winter
Fronts
NSTF (Northern Subtropical Front)
AF (Agulhas Front)
SSTF (Southern Subtropical Front)
SAF (Subantarctic Front)
PF (Polar Front)
Oceanic Zones
Tropical
Subantarctic
North subtropical
Polar Frontal
South subtropical
Antarctic

Figure 8